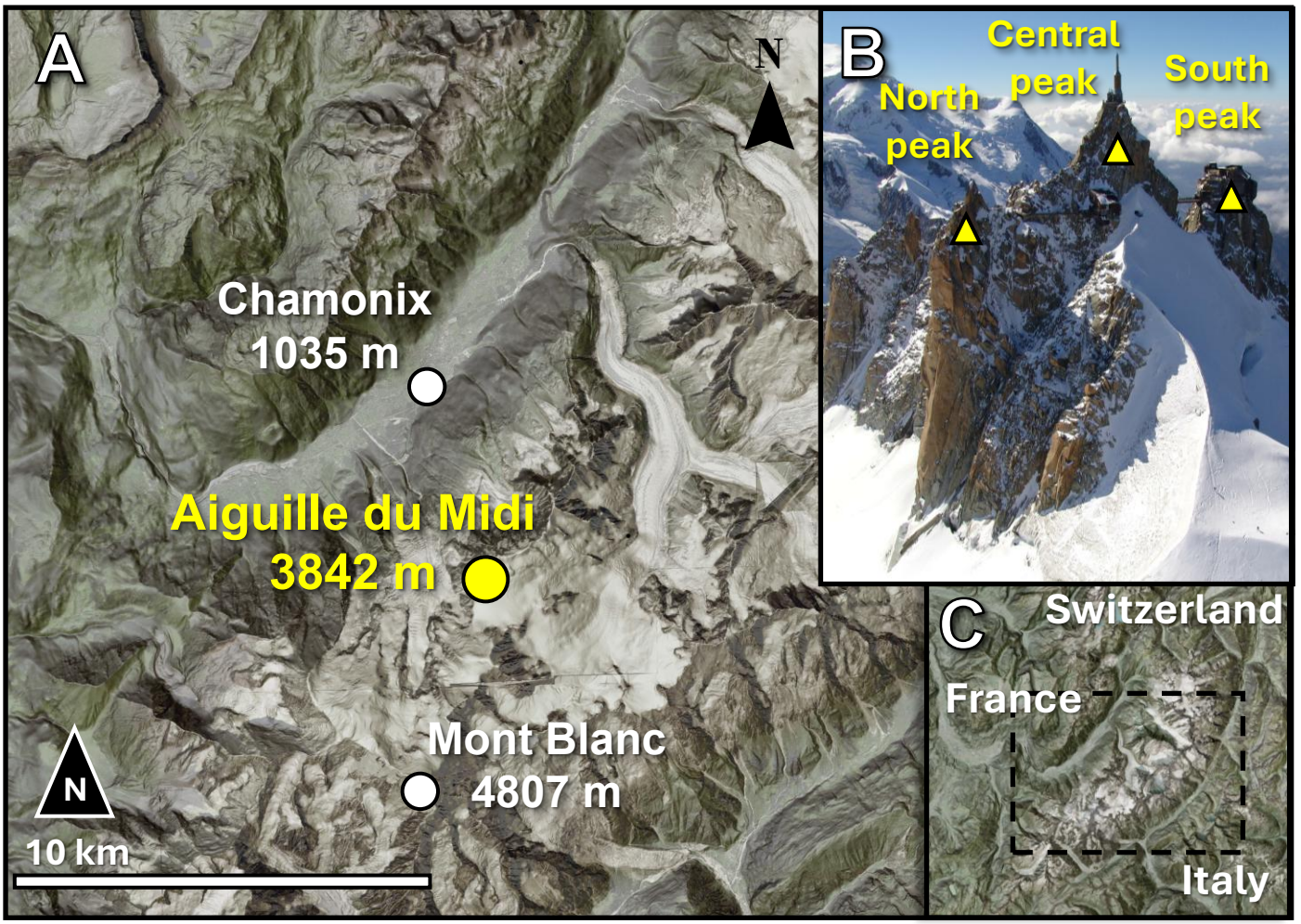

Figure 1: A) Location of the Aiguille du Midi in the Mont Blanc massif. B) view of the three peaks at Aiguille du Midi. (Picture: S. Gruber). C) Location of the Mont Blanc massif on the border of France, Italy and Switzerland. Maps provided by the Swiss Federal Office of Topography swisstopo.

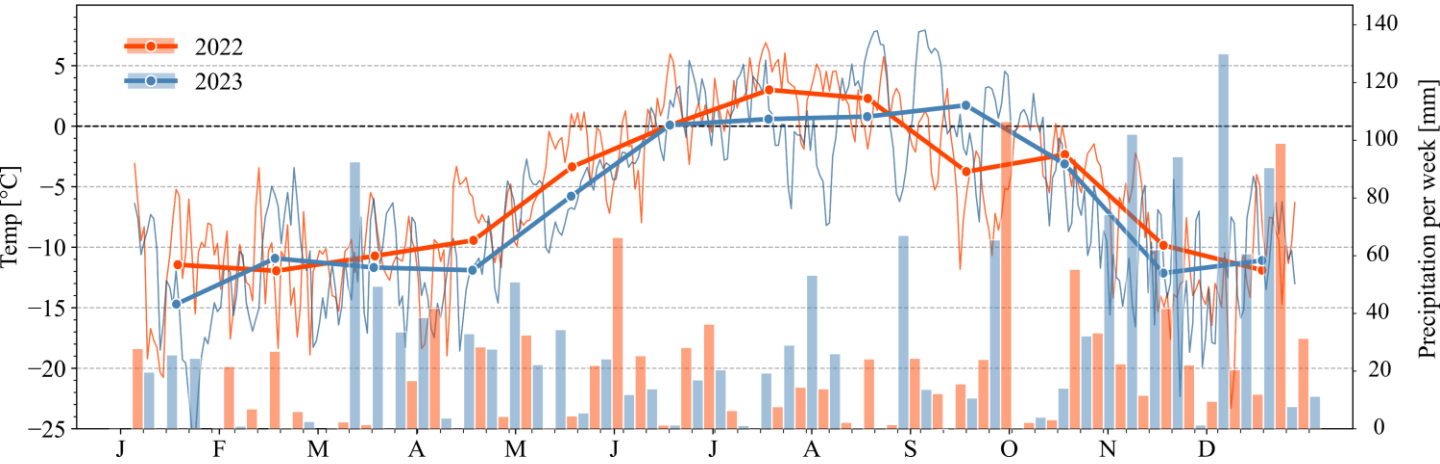

Figure 2: Daily (thin lines) and monthly (thick lines) air temperature and weekly precipitation in 2022 and 2023 (bars). Air temperature was measured at the top of the Aiguille du Midi and precipitation was measured in Chamonix (1042 m asl). Data provided by Météo France.

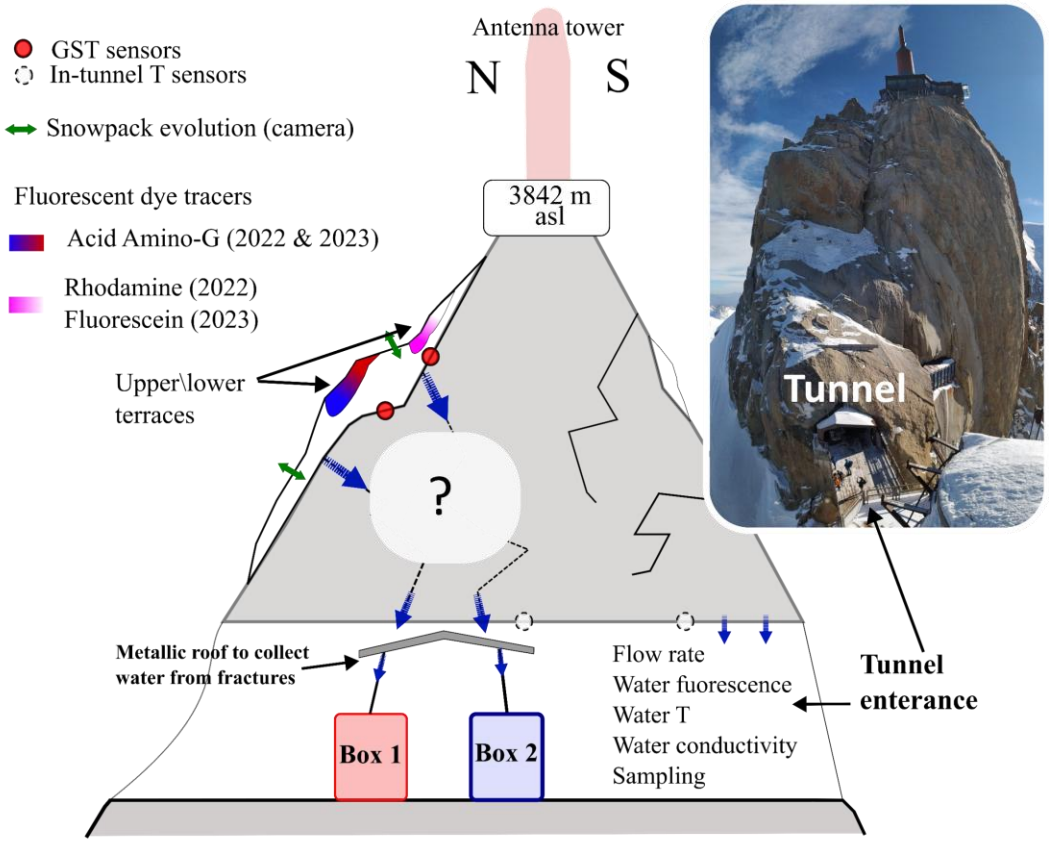

Figure 3: Sketch of the methodological approach to track and monitor water flows in the Aiguille du Midi central pillar. Note the location of the insertion locations of the dye tracers in the snowpacks on the terraces above the water monitoring boxes.

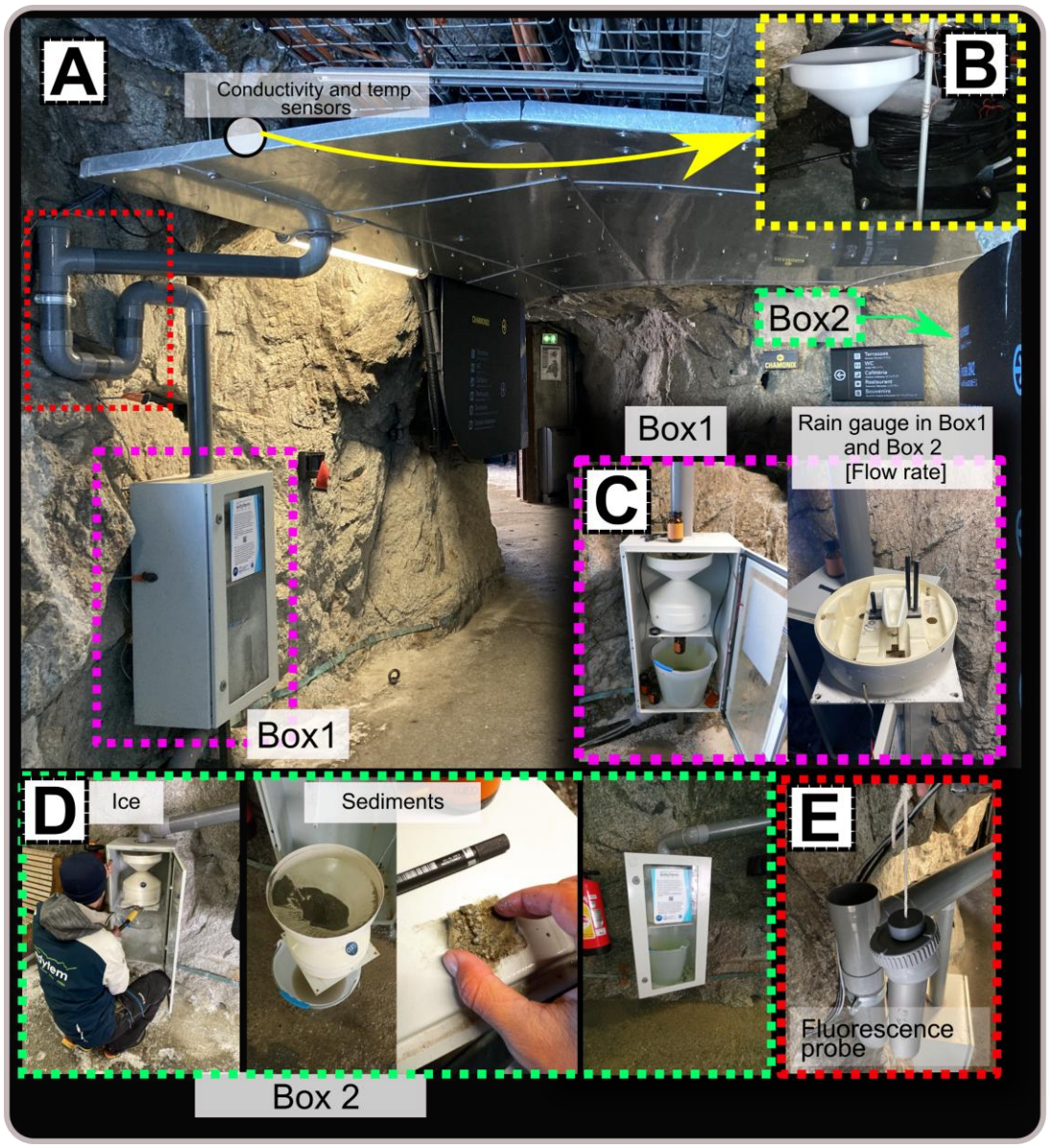

Figure 4: Real-time monitoring system in the tunnel. A) The metal roof that drains to Box 1 (pink dashed frame). Originally installed to divert meltwater flowing out of fractures from dripping on visitors. B) A 3D printed siphon that was placed directly under the water output from the fracture, equipped with temperature and conductivity sensors (yellow dashed frame). C) Box 1 interior with a rain gauge to monitor flow rate, a sampling bottle, and a bucket. D) Box 2 with sediments (green dashed frame). E) Fluorescence probe by TRAQUA located in a specially designed siphon for continuous real-time monitoring of the dye tracers.

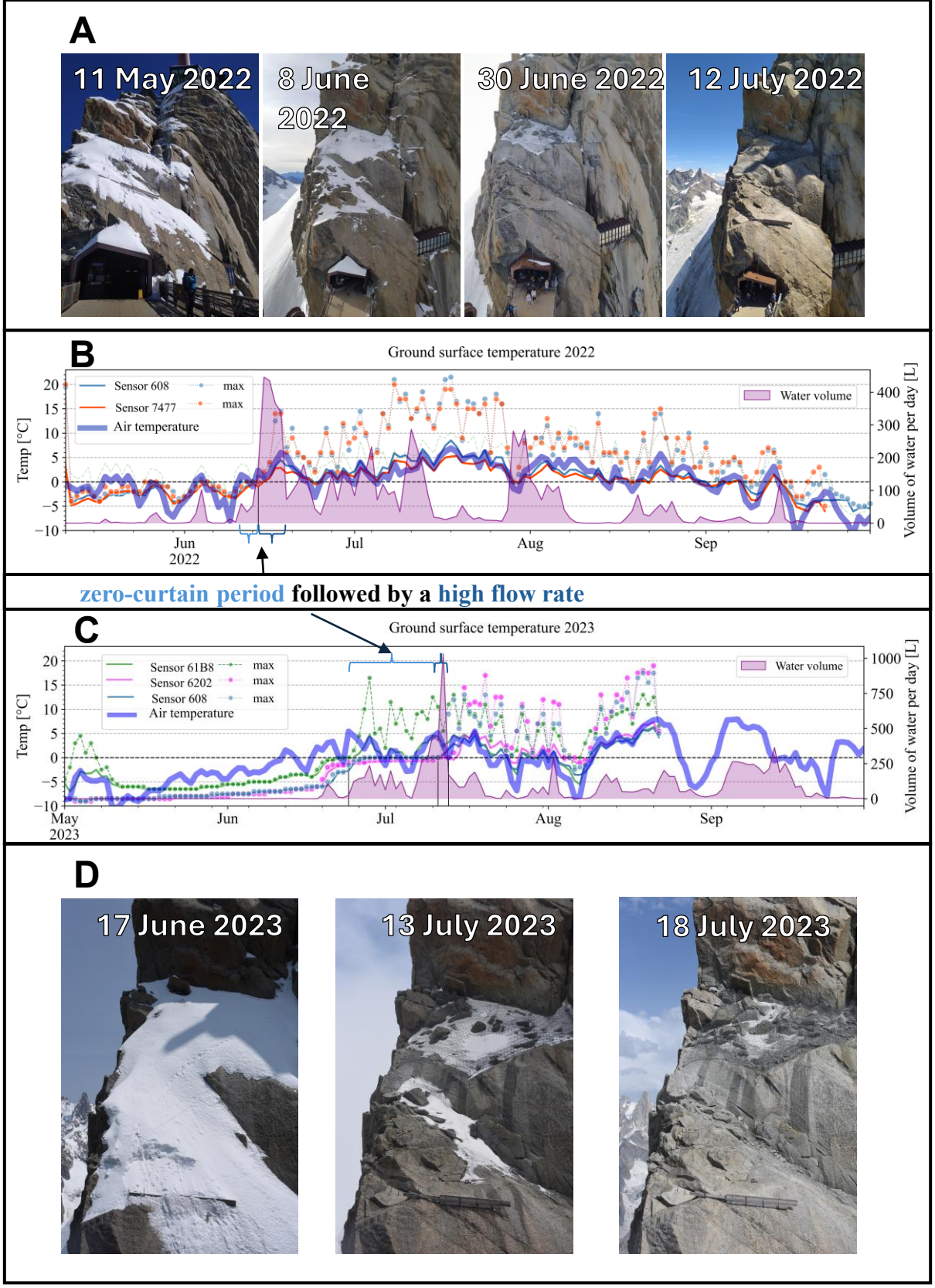

Figure 5: A) Photos showing the evolution of the snow cover on the NE face during the snow melt season in 2022. Note the change in snow cover. B) 2022 season AT, GST measured on the NE face, above the tunnel entrance, directly above the monitoring system, and flow rate measured at the output from rock fractures in the tunnel wall. Solid lines represent the daily mean. C) 2023 season AT, GST measured on the NE face, above the tunnel entrance, directly above the monitoring system, and flow rate measured at the output from rock fractures in the tunnel wall. Solid lines represent the daily mean. Note the zero-curtain period, which marks the melting of the snowpack and the exposure of the rock surface to atmospheric heating. D) Photos showing the evolution of the snow cover on the NE face during the snow melt season in 2023.

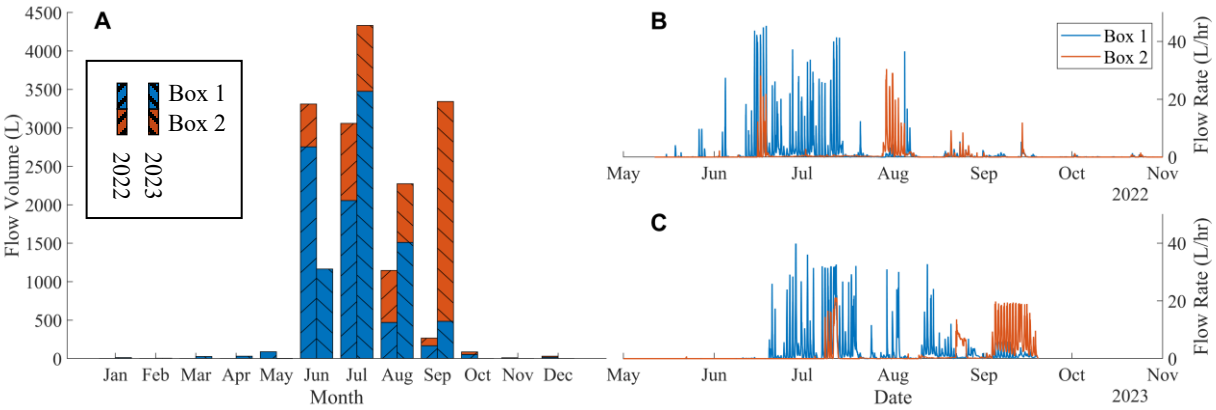

Figure 6: A) Monthly distribution of flow volume in Box 1 and Box 2 during the 2022 and 2023 seasons. B) Measured flow rate vs. time in 2022. C) Measured flow rate vs. time in 2023.

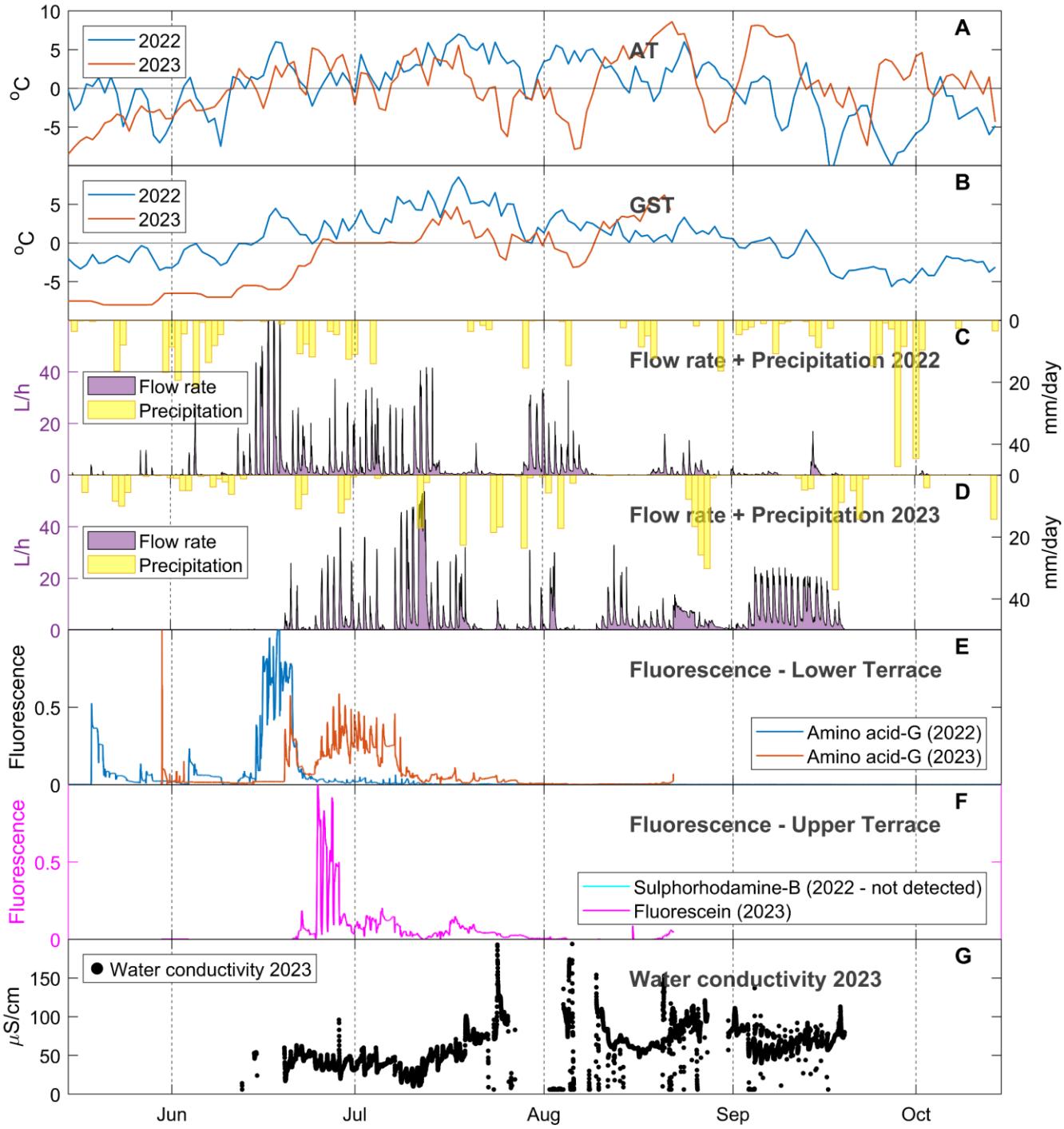

Figure 7: Annual time series. A) Air temperature (AT) measured by Météo-France in Aiguille du Midi. B) Ground surface temperatures (GST) measured using iButtons at the rock surface on rock slope above the water collecting system, near the location of fluorescent dyes injection. C-D) Flow rate measured in both box 1 + box 2 (purple) and daily precipitation measured in Chamonix meteorolocical station (Météo-France) (yellow bars). E) Normalized fluorescence signal of amino acid-G dye tracer that was inserted in the upper terrace in both seasons (2022 and 2023). F) Normalized fluorescence signal of Sulphorhodamins-B (inserted in 2022) and Fluorescence (inserted in 2023) dye tracers. The Sulphorhodamins-B dye was never detected. G) Water conductivity that was monitored continuously at the outlet of water from the fracture in the tunnel.

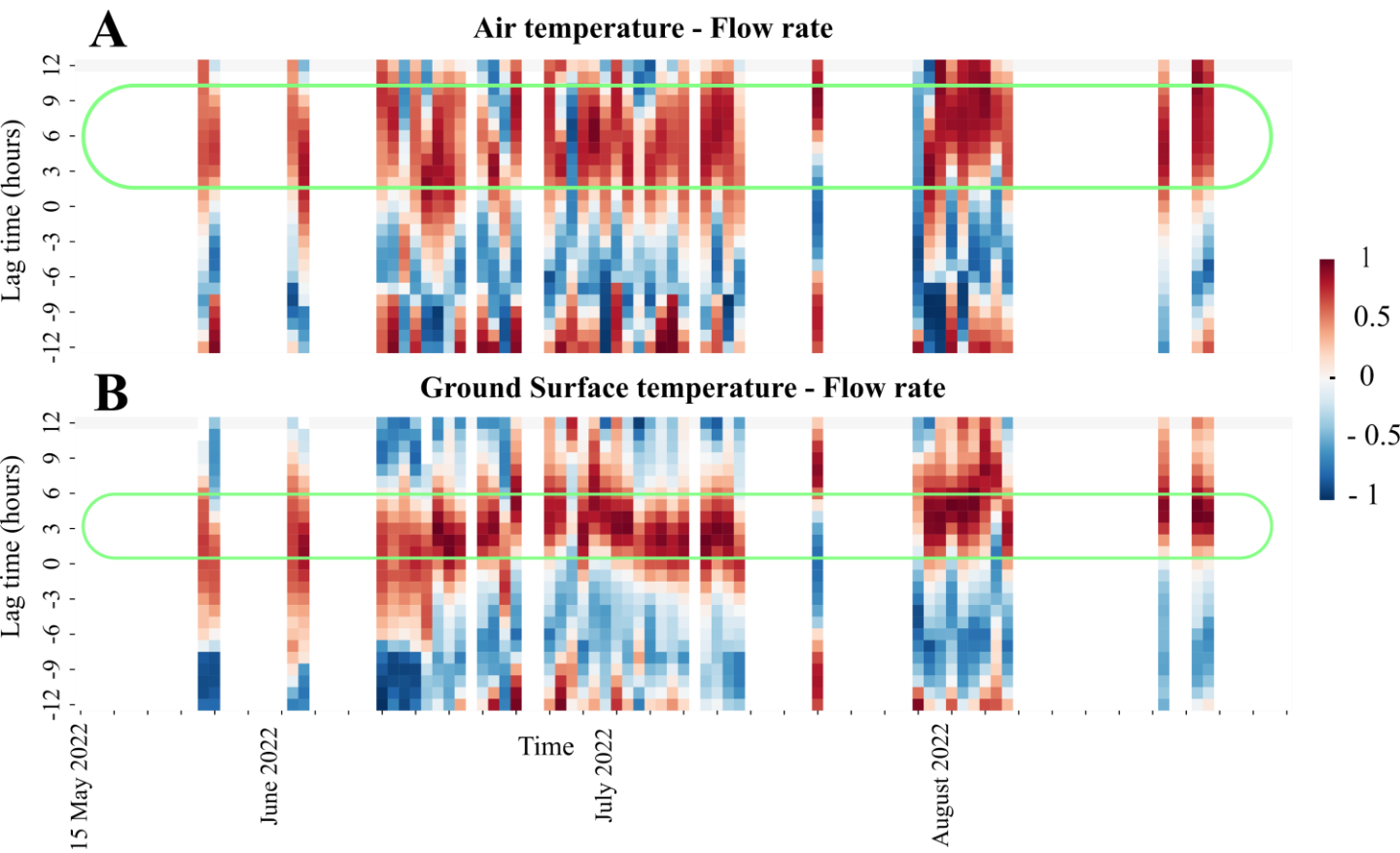

Figure 8: Results of moving-window cross-correlation analysis of water flow with (A) air temperatures (AT) and (B) ground surface temperatures (GST), during 2022 season. The horizontal axis represents the days, and the vertical axis represents the size of the lag time, in hours, between the flow rate time series with AT (upper plot) and GST (lower plot). The color bar represents the value of the Pearson correlation coefficient (PCC) (1: high correlation, 0: no correlation, -1: reverse correlation). The green frame marks the range of lag times that show high PCC. Results of the cross-correlation analysis of 2023 season show similar results and can be found in the supplementary materials, in figure S3.

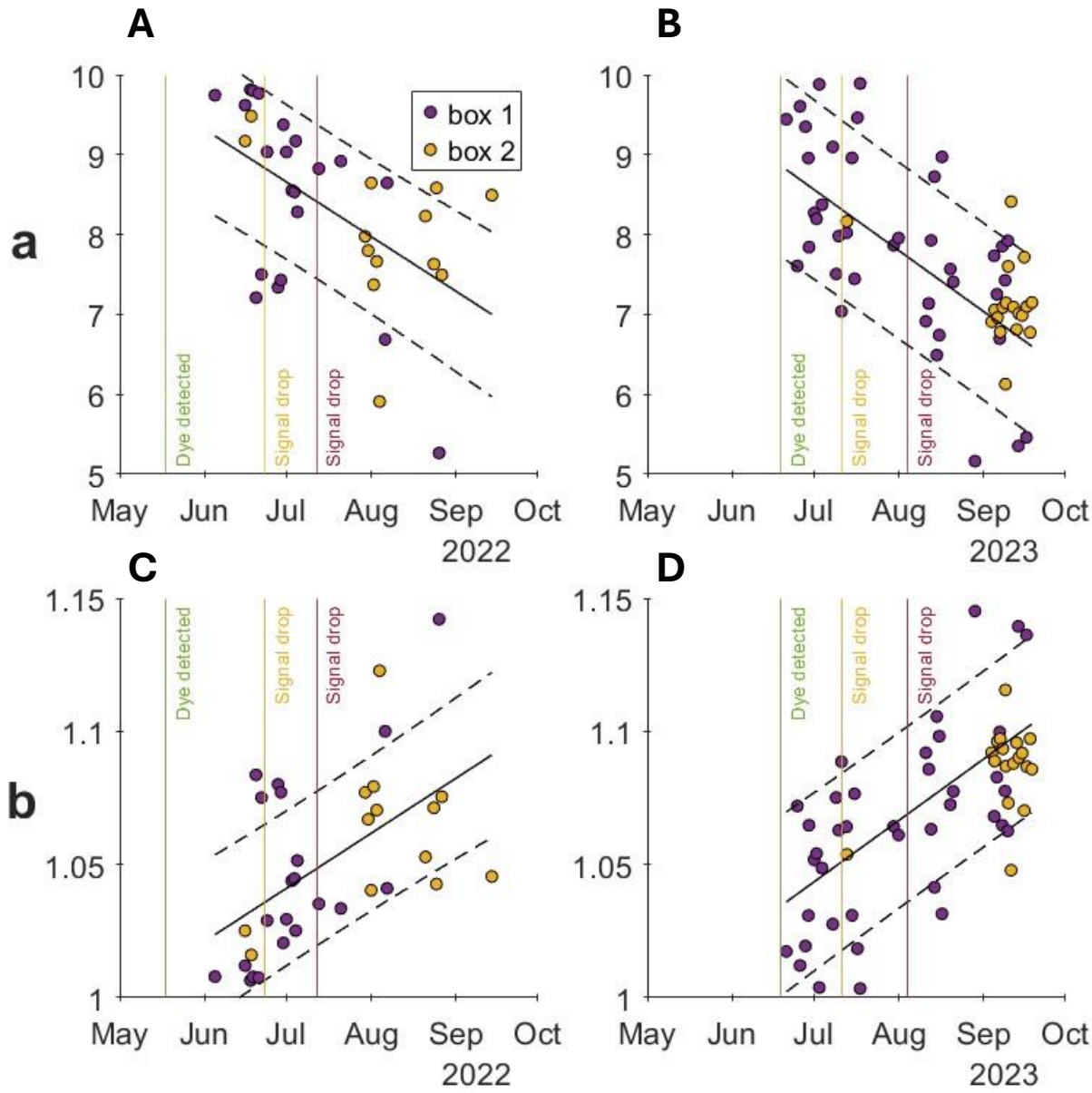

Figure 9: Values of the recession curve exponential coefficients a (top) and b (bottom) in 2022 (left) and 2023 (right) vs. time. A) values of the 'a' coefficient of the recession curves of flow events in 2022 in box 1 (purple circles) and box 2 (yellow circles). B) values of the 'a' coefficient of the recession curves of flow events in 2023 in box 1 (purple circles) and box 2 (yellow circles). C) values of the 'b' coefficient of the recession curves of flow events in 2022 in box 1 (purple circles) and box 2 (yellow circles). D) values of the 'b' coefficient of the recession curves of flow events in 2023 in box 1 (purple circles) and box 2 (yellow circles). Values obtained from curves with R^2 values below 0.8 were omitted from the analysis. The black line is the linear regression of all the points (box 1 + box 2) with ±standard error (dashed black lines). The vertical lines indicate the timing of the detection of the fluorescent dye in the water that exits the fractures (green), the rapid drop of the signal intensity (orange), and the disappearance of the signal (red).

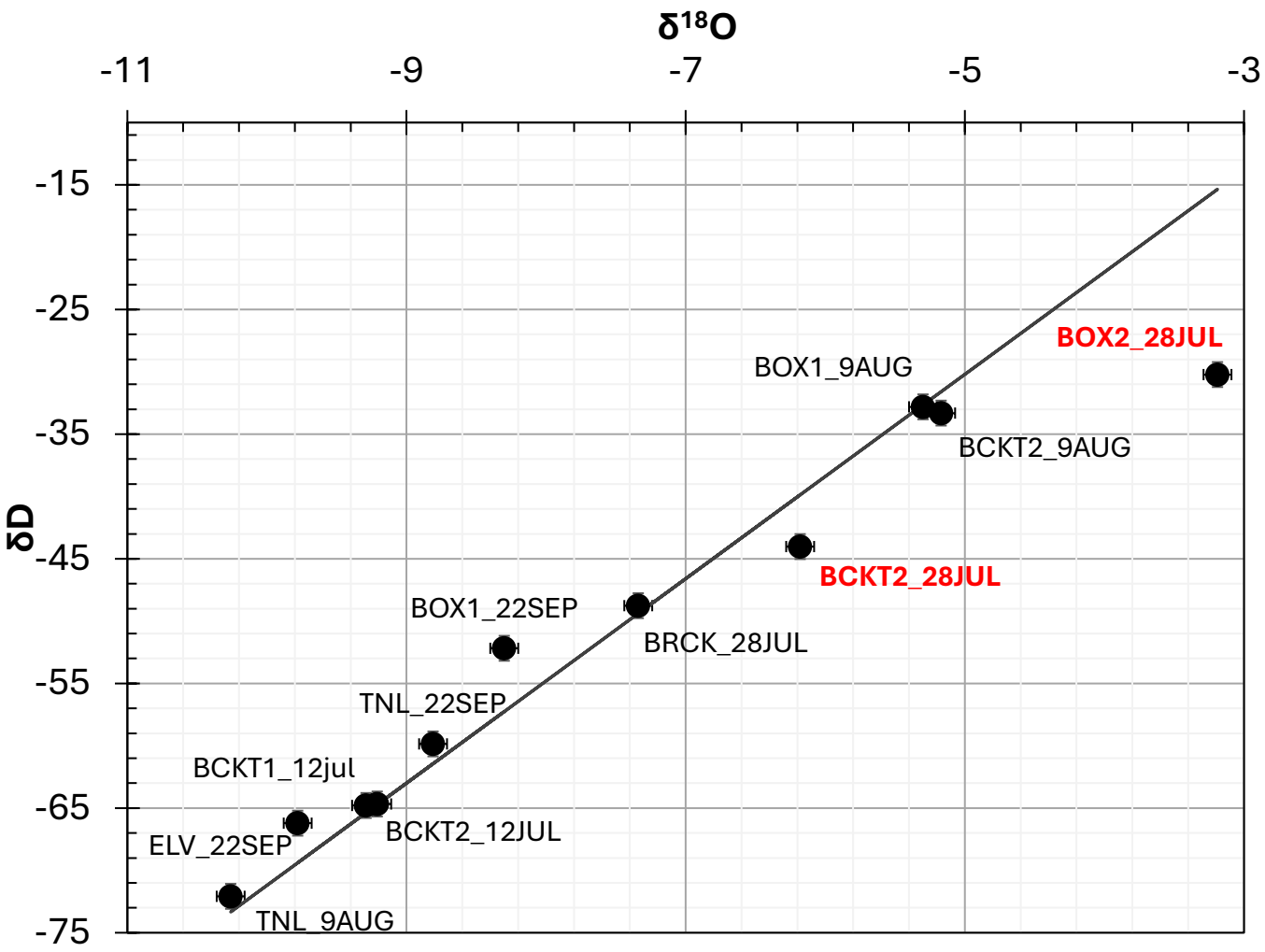

Figure 10: Stable isotopes $\delta^{18}O$ and δD in water samples. Note the two outliers (labeled in red) from the global meteoric water line (GMWL, black line) in samples taken from Box 2 on 28 July 2022.

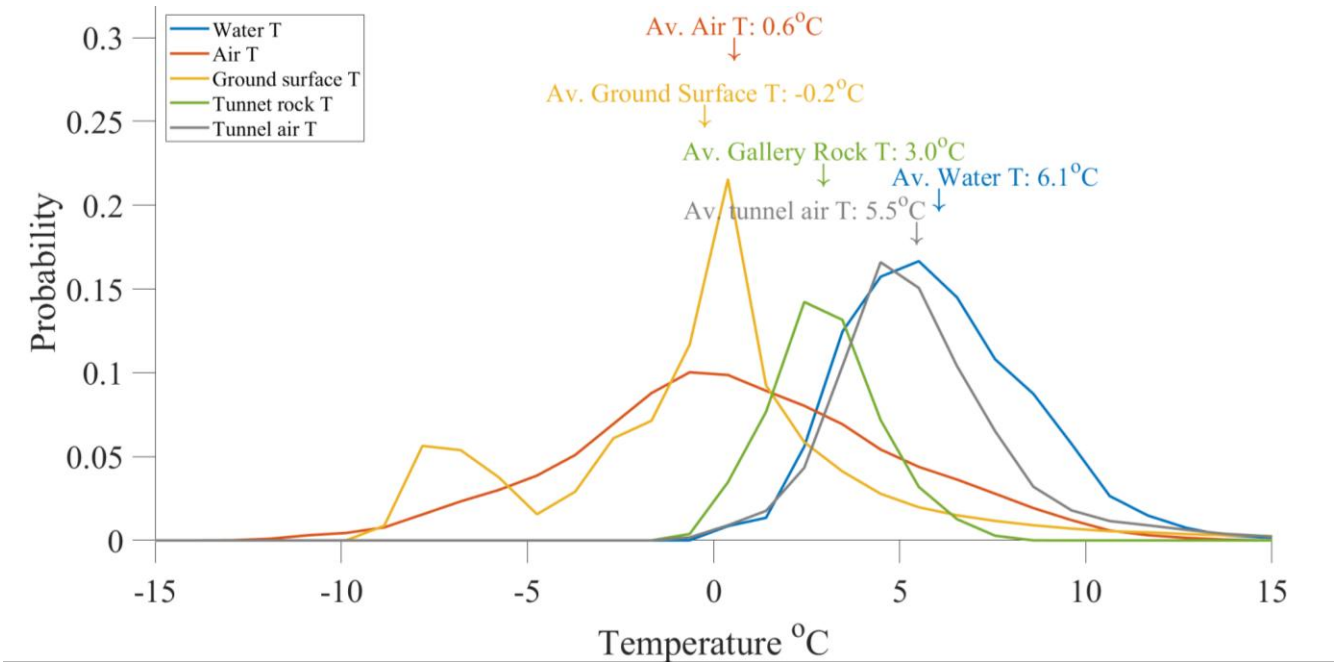

Figure 11: Probability distribution of temperatures monitored during flow events (blue), atmospheric ATs (orange), ground surface temperatures (yellow), and tunnel wall (green). All distributions show data from the thawing season in 2022 and 2023 (15 May – 15 September). Note that the water temperature distribution (blue) shows only data when water flow was detected in the monitoring system, while the other temperature distributions represent the entire data within the thawing season.